Polarization Imaging Applied to 3D Reconstruction of Specular Metallic Surfaces

Olivier Morel, Fabrice Meriaudeau, Christophe Stolz, and Patrick Gorria
Le2i - CNRS UMR5158, 12 rue de La Fonderie, 71200 Le Creusot, France

ABSTRACT

This paper presents a new application of "Shape from Polarization" method to specular metallic surfaces. It demonstrates how to extend the commonly used method for dielectric to metallic surfaces. Studying the state of polarization of the reflected light is very useful to get information on the normals of the surface. After computing the surface normals, the 3D surface is reconstructed thanks to a relaxation algorithm. Applications on shape defects detection are discussed, and the efficiency of the system to discriminate defects on metallic objects made by stamping and polishing is presented.

Keywords: Polarization imaging, specular metallic surfaces, 3D inspection, 3D reconstruction

1. INTRODUCTION

The 3D machine vision systems market is expanding rapidly, providing 3D-based machine vision for process control. Nevertheless, the inspection of specular metallic objects remains a delicate task, since it implies to control the whole lighting of the scene. Extracting the shape information of specular metallic surfaces from a single view is still a challenging problem, and there are currently two kinds of techniques. The first one is to study the highlights of structured lightings, with multiple ring lights[1], with a hemisphere of 127 points sources like the SHINY system[2], or with a calibrated pattern composed of lines[3, 4]. The second technique is to study the motion of a specularly reflected pattern on the surface which is different of the real motion of the object[5]. We propose a new way of reconstructing the 3D information on specular metallic objects, by extending the "Shape from Polarization" method to metallic surfaces. The aim is to reveal the shape defects on decorations from metallic objects made by stamping and polishing (Fig. 1). Seulin[6] has previously developed a dynamic lighting by projecting a fringes pattern to detect geometric aspect surface defects. The defects are revealed near the transition between a dark fringe and a bright fringe as shown on Fig. 2a. By moving the lighting, and thanks to a saturated camera, the system brings an aspect image where the defects can be efficiently segmented (Fig. 2b). Nevertheless, Fig. 2b, also shows that this system is not adapted to inspect the shape defects on the object decorations. Therefore, we propose a complementary process to resonstruct the 3D shape of the decorations based on the "Shape from Polarization" method. This method was especially developed by Miyazaki[7, 8], and Rahman[9, 10] for transparent or reflective surfaces, but of dielectric nature. By using the complex refractive index of the surface, we've found new relations between the polarization images and the surface normals. Once the surface normals are computed, the surface is reconstructed by integration.

The paper is organized as follow: the principle of "Shape from polarization" for dielectric surfaces is reminded in section 2. In section 3, the extension to metallic surfaces is developed, and the integration algorithm is also provided. The description of the acquisition system, and the results are exposed in section 4.

2. POLARIZATION IMAGING

The polarization imaging enables to study the polarization state of a light wave. For instance, this technology can be used in industrial vision, to distinguish dielectrics and metallics[11]. The polarization imaging enables likewise to reconstruct the 3D shape of simple objects thanks to the reflection or refraction study of an unpolarized light wave: the so called "Shape from Polarization" method. The physical principle used is the following: after being reflected, an unpolarized wave becomes partially linearly polarized, depending on the surface normal and on the refractive index of the media it impinges on. This section firstly describes how to study a partially linearly polarized wave, and secondly, it reminds the "Shape from Polarization" method.

Further author information: (Send correspondence to O.M.)
O.M.: E-mail: o.morel@iutlecreusot.u-bourgogne.fr

Figure 1. Zoom on decorations from metallic objects.

(a) (b)

Figure 2. Defects detection with the dynamic lighting: (a) One frame of the acquisition system, and (b) Aspect image.

2.1. Partial linear polarization state of a light wave

To study the polarization state of a partially linearly polarized light wave, Wolff[12] considers it as the sum of two components: a completely linearly polarized light wave, and a completely unpolarized light wave. Therefore, a polarization sensor has to be able to compute the magnitude of the light, the proportion of the polarized component, and the angle of the linearly polarized component. A natural way to set up this sensor, is to use a rotating polarizer in front of a camera. To speed up the sensing of polarization components, the polarizer can also be replaced by liquid crystals systems[13].

The relationship between the magnitude I_p of the transmission of a partially linearly polarized light wave through a rotating polarizer, and the angle α of the polarizing filter is given by a sinusoid, as shown in Fig. 3.

This relation can be written in the form:

$$I_p(\alpha) = \frac{I_{max} - I_{min}}{2} \cos(2\alpha - 2\varphi) + \frac{I_{max} + I_{min}}{2}, \tag{1}$$

where I_{min} and I_{max} represent, respectively, the minimum and the maximum magnitude seen through the polarizer. The magnitude of the light I, and the proportion of the polarized component ρ (also called the degree

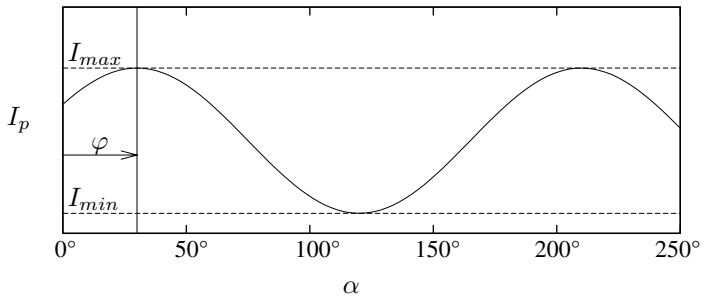

Figure 3. Variation of the light intensity according to the angle of the polarizer.

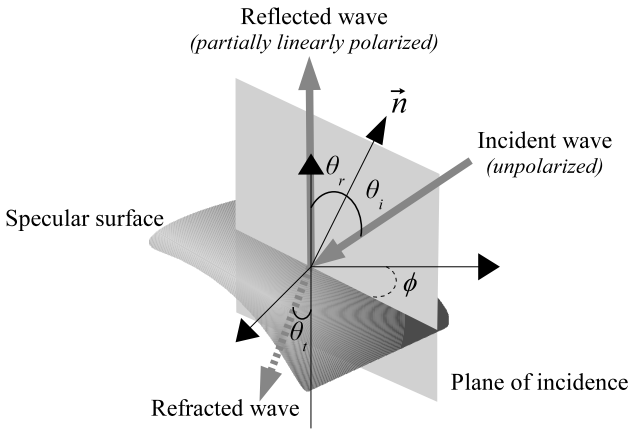

Figure 4. Reflection of a light wave on a specular surface.

of polarization), can be derived from equation (1) according to:

$$I = I_{max} + I_{min}, \qquad \rho = \frac{I_{max} - I_{min}}{I_{max} + I_{min}}. \tag{2}$$

The third parameter of the partially linearly polarized wave, is the angle of the linearly polarized component φ which is simply given by the phase shift of the sinusoid. The purpose of polarization imaging is to compute the three parameters: I, φ, and ρ, by interpolating the formula (1). There are several methods to fit the equation in order to get the parameters. Because, there are three parameters, we need at least to take three images with different orientation of the polarizer. For instance, Wolff[13] takes three images I_0, I_{45}, and I_{90} corresponding to three orientations of the polarizer equal to $\alpha = 0°$, $45°$, and $90°$. The main advantage of this method, is that images of the parameters can be computed in real time but it is very noise sensitive. Since the degree of polarization is lower for metallic surfaces, and to improve the accuracy of the measure of the parameters, the linear least squares method is applied by taking 18 frames with a constant step of 10 degrees.

2.2. Principle of "Shape from Polarization"

Wolff[14] has demonstrated how to determine constraints on surface normals by using the Fresnel reflectance model. This method is also adapted to highly reflective surfaces. Fig. 4 shows the specular reflection of an unpolarized light wave on a surface.

The Fresnel coefficients of reflection $F_\perp$and $F_\parallel$, are the ratio between the amplitude of the reflected light and the incident light, according respectively to the perpendicular and the parallel plane to the plane of incidence:

$$\left.\begin{array}{l} F_\perp = \frac{\sin^2(\theta_i - \theta_t)}{\sin^2(\theta_i + \theta_t)}, \\ F_\parallel = \frac{\tan^2(\theta_i - \theta_t)}{\tan^2(\theta_i + \theta_t)}, \end{array}\right\} \tag{3}$$

where θ_i is the angle of incidence, and θ_t is the angle of refraction.

2.2.1. Relationship between the angle of polarization φ and the plane of incidence ϕ

The Fresnel formulae (3) show that the orthogonal component $F_\perp$ is greater than the parallel one $F_\parallel$. Therefore, it means that an unpolarized light wave becomes partially linearly polarized according to the normal of the plane of incidence. Thus, by determining the angle of polarization φ, we are able to deduce the orientation of the plane of incidence: $\phi = \varphi \pm \frac{\pi}{2}$.

2.2.2. Relationship between the degree of polarization ρ and the angle of reflection θ_r

The disparity between the components $F_\perp$ and $F_\parallel$ brings also a new piece of information: the degree of polarization of the reflected light. By denoting I_{min} and I_{max} , the minimum and the maximum magnitude of the light wave through a rotating polarizer, we have:

$$\left.\begin{aligned} I_{max} &= \tfrac{F_\perp}{F_\perp+F_\parallel} I, \\ I_{min} &= \tfrac{F_\parallel}{F_\perp+F_\parallel} I. \end{aligned}\right\} \tag{4}$$

Thus, the degree of polarization defined in equation (2) can be expressed as:

$$\rho = \frac{F_\perp - F_\parallel}{F_\perp + F_\parallel}. \tag{5}$$

Moreover, by denoting n the relative refractive index between the object and the air, the Snell-Descartes's law gives:

$$\sin\theta_i = n \sin\theta_t, \tag{6}$$

By substituting equation (3) into equation (5) with Snell-Descartes's law, and by writing $\theta = \theta_r = \theta_i$, the degree of polarization ρ can be expressed as:

$$\rho(\theta) = \frac{2\sin\theta\tan\theta\sqrt{n^2 - \sin^2\theta}}{n^2 - 2\sin^2\theta + \tan^2\theta}. \tag{7}$$

This equation gives the relationship between the angle of reflection θ and the degree of polarization ρ for dielectric surfaces.

3. EXTENSION TO METALLIC SURFACES

This section describes our main contributions concerning the "Shape from Polarization" method extended to metallic surfaces, and the integration algorithm.

3.1. Use of the complex refractive index

Unfortunately, the relation (7) can not be directly applied to metallic surfaces since their refractive indexes are complex. The complex index $\hat{n}$ can be generally written in the form: $\hat{n} = n(1 + i\kappa)$ where κ is called the attenuation index. In this case, the Snell-Descartes equation (6) implies that the refractive angle θ_t is complex. Therefore, the Fresnel coefficients are given by:

$$\left.\begin{aligned} F_\perp &= \left|\tfrac{\sin(\theta_i-\theta_t)}{\sin(\theta_i+\theta_t)}\right|^2, \\ F_\parallel &= \left|\tfrac{\tan(\theta_i-\theta_t)}{\tan(\theta_i+\theta_t)}\right|^2. \end{aligned}\right\} \tag{8}$$

In order to simplify the relations, and as it is usually the case in the visible region, we apply the following approximation[15]:

$$|\hat{n}|^2 = n^2(1 + \kappa^2) \gg 1. \tag{9}$$

In the same way, and thanks to the approximation, we find an inversible relation in the form:

$$\rho(\theta) = \frac{2n\tan\theta\sin\theta}{\tan^2\theta\sin^2\theta + |\hat{n}|^2}. \tag{10}$$

The difference between the true degree of polarization and its approximation grows slightly only for great values of the angle θ (Fig. 5).

The curve also shows that the ambiguity concerning the determination of the angle θ, according to the degree of polarization ρ, doesn't have do be treated for surfaces with slopes lower than 75°, as it is usually the case with the studied objects.

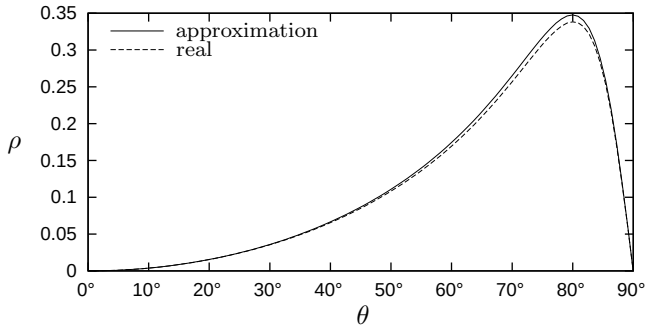

Figure 5. Comparison between the approximated degree of polarization and the real degree of polarization for a metallic surface ($\hat{n} = 1.94(1 + 2.7i)$).

3.2. Surface reconstruction

We make the assumption that the surface is a Cartesian one, defined by $z = f(x, y)$. The normal in each point is given by:

$$\overrightarrow{n} = \begin{vmatrix} -\frac{\partial f(x,y)}{\partial x} \\ -\frac{\partial f(x,y)}{\partial y} \\ 1 \end{vmatrix} = \begin{vmatrix} p = tan\theta cos\phi \\ q = tan\theta sin\phi \\ 1 \end{vmatrix} . \tag{11}$$

This expression enables to assume the link between the normal and the derivative of each point of the surface. Since, the angles θ and ϕ, are computed thanks to polarimetric images, the goal is to determine $z = f(x, y)$ by integrating. In order to keep the continuity between the rows and the columns of the image, a relaxation algorithm based on Taylor's approximations is applied:

$$f_{n+1}(i, j) = \frac{1}{S} H(i, j) * f_n(i, j) + \frac{a \cdot \epsilon^2}{2S} \left(\frac{\partial p}{\partial i} + \frac{\partial q}{\partial j} \right), \tag{12}$$

where S is the sum of the H filter coefficients, ϵ represents the step between each pixel, and a is given by:

$$a = \sum_{u=-k}^{k} \sum_{v=-k}^{k} H(u, v)u^2 = \sum_{u=-k}^{k} \sum_{v=-k}^{k} H(u, v)v^2. \tag{13}$$

Moreover, H has to be a $2k + 1$ by $2k + 1$ smoothing filter with the following constraints:

$$\forall (u, v) \in [-k, k]^2 \, , \, H(u, v) = H(-u, v) = H(u, -v). \tag{14}$$

The iterative relation (12) is a general formulation of the standard relaxation algorithm[16]. It enables to use larger filter in order to increase the convergence of the reconstruction algorithm. The algorithm is initialized by a reference plane extracted from a surface in which the decorations of the object don't appear.

4. APPLICATION AND RESULTS

4.1. Experimental set up

The acquisition system is made of a CCD camera, a liquid crystal polarization rotator, and a diffuse dome light (Fig. 6). The diffuse dome light is used to provide an unpolarized light on the whole surface. After reflection the light which becomes partially linearly polarized is studied with the liquid crystal polarization rotator and the camera. The liquid crystal polarization rotator acts like a rotating polarizer which can be electrically controlled.

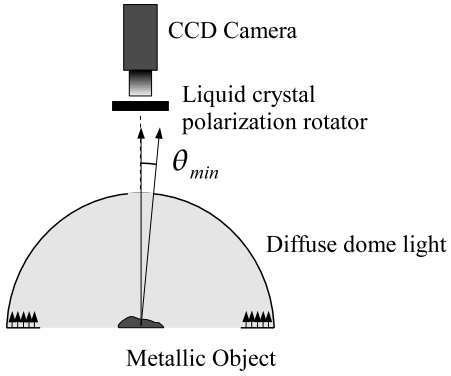

Figure 6. Experimental set up.

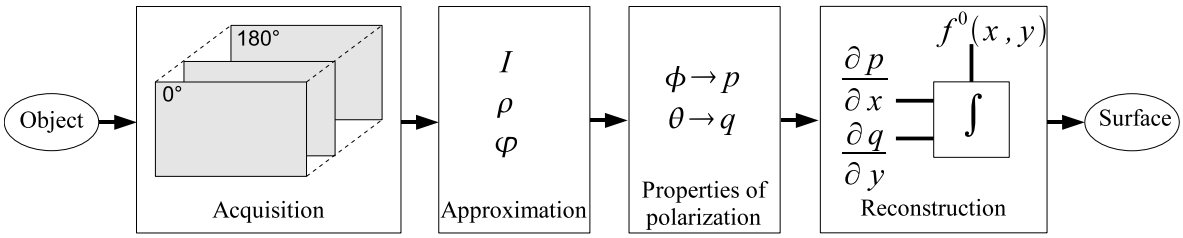

Figure 7. Whole process of image processing.

This device uses nematic liquid crystal cell associated with a linear polarizer, and a quarter wave plate, which provides tunable polarization by changing the supplied voltage. Since the degree of polarization is lower for metallic surfaces, we use a sensitive camera with 10 bits depth. A limitation of our system is due to the hole for the camera, leading to a θ_{min} value which is about 3°. Therefore, the object has to be correctly oriented in order to respect the constraints about the angle θ. Nevertheless, approximating the angle θ inferior than 3° to $\theta = 0°$ (a normal orientation) doesn't lead to a significant error of the 3D surface reconstruction.

Because of the manufacturing process, the metallic objects we're working on, are provided with different shape details and 3D information have to be extracted. The decorations of the objects are made by stamping, meaning the slopes don't exceed 75°. Moreover, the objects are polished in order to get the surfaces of polish mirror quality, therefore the reflections are assumed to be specular. To initialize the 3D reconstruction process, a plane is given from the theoretical surface without the decorations. The whole process of image processing is summed up in Fig. 7.

The 18 Frames are acquired with different rotations of the polarization rotator from 0 to 180°, with a constant step of 10°. The least mean square method is applied during the acquisition process, while the polarization rotator is turning. Therefore, it takes less than one second to acquire the 18 images, and to compute the three parameters of polarization (Fig. 8) by fitting the sinusoid. By knowing the object's complex index of refraction, the surface is reconstructed from the initialization plane according to the presented iterative algorithm (12). Our system can also be used to estimate the refractive index of the object surface with the opposite method: from a known surface, the degree of polarization leads to the refractive index (equation (10)).

4.2. Results

In order to qualitatively compare the 3D surface obtained with our system to a 3D surface of reference, the object was scanned with a 3D scanner (Replica 500). This scanner based on laser ranging, takes regular points with step of $50\mu m$ in X and Y axis, and the precision in Z axis is about $20\mu m$. Since such a scanner is sensitive to the reflectivity of surface, a thin opaque coating has to be applied onto the object. Consequently the details of the object appear clearly more marked with our method rather with the scanner (Fig. 9a and Fig. 9b).

(a) Intensity (b) Degree of polarization (c) Angle of polarization

Figure 8. Parameters of polarization.

After registering the 2 surfaces, the mean deviation between the surfaces is about $30\mu m$, meaning that the shape is qualitatively well reconstructed. Moreover, the cross section (Fig. 9c) highlights the good accuracy of the surface computed with our method. The resolutions along the axis X and Y depend only on the used lenses and on the spatial resolution of the sensor: for instance, we are able to get X, Y resolutions 3 times finer. Thus, "Shape from polarization" extended to metallic surfaces presents encouraging preliminary results, and our method can be easily integrated into an automatic process of shape defects detection.

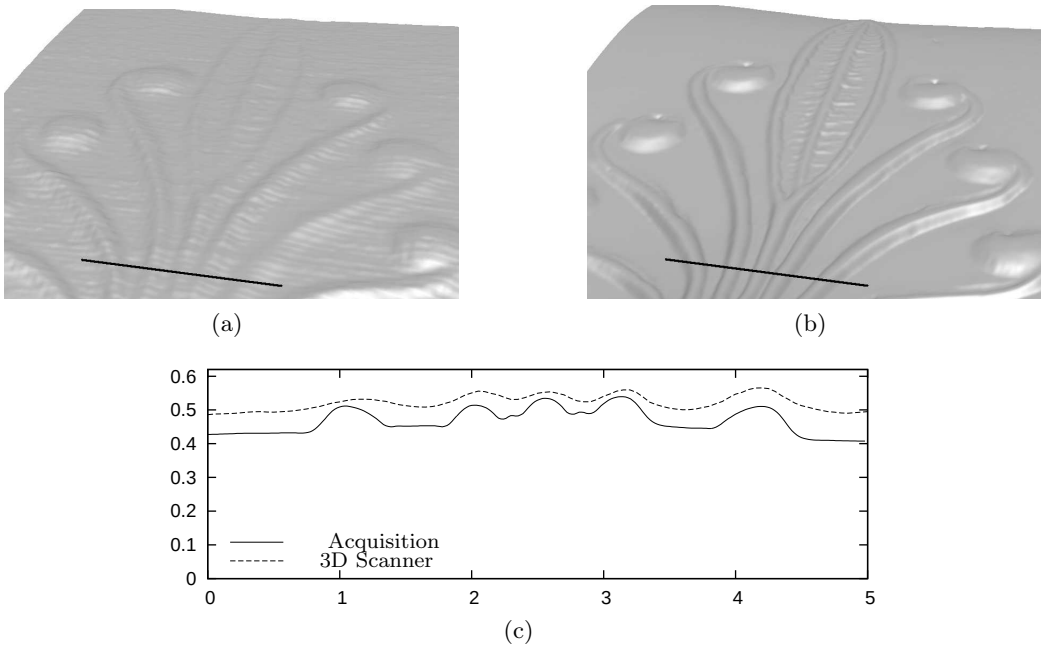

(a) (b)

(c)

Figure 9. Reconstruction of the 3D surface of a metallic object: (a) Surface from the 3D scanner, (b) Surface from our method, and (c) Comparison of the cross sections (scales given in mm).

4.3. 3D inspection

The aim of our system is to inspect specular metallic objects. The Fig. 10 illustrates the 3D surface reconstruction for two objects: a reference one and one with a shape defect on the left-bottom "bump".

After an automatic registration of the two shells, the mean deviation between the surfaces is computed (Fig 10e). The comparison shows the efficiency to discriminate the shape defect.

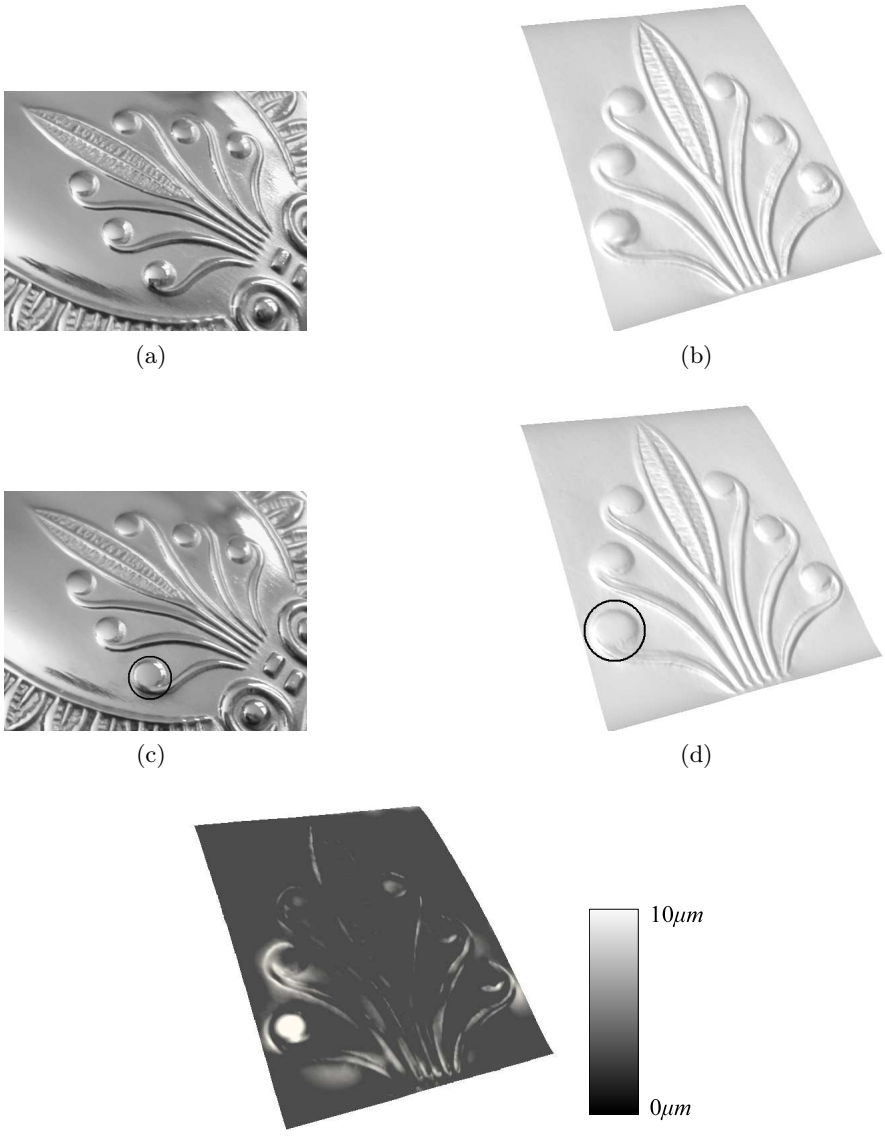

Figure 10. Polarization imaging applied to 3D reconstruction of specular metallic objects: (a) Object of reference photograph and its 3D reconstructed surface (b). (c) Object with a shape defect photograph, and its 3D reconstructed surface (d). (e) Mean deviation map between the surfaces (b) and (d).

5. CONCLUSION AND FUTURE WORKS

In this paper, a new way of reconstructing the 3D surface of specular metallic objects is presented. The method of "Shape from Polarization" has been extended to specular metallic surfaces, in order to detect shape defects on objects made by stamping and polishing. The involved process is quite simple, requiring a diffuse dome light, a CCD camera and a polarization rotator. The polarization imaging enables to compute the normals surface, then the 3D surface is obtained by integrating the normals thanks to a relaxation algorithm. The comparison between the 3D surface and the surface obtained by a 3D scanner shows qualitatively the efficiency of our method to reconstruct the objects shape. Moreover, the comparison between two surfaces reconstructed from a reference object and an object with a shape defect enables to reveal the defect. The acquisition process and the polarization images extraction takes less than one second. The integration process time has to be reduced in order to integrate the whole system into an automatic process. Therefore, future works will consist in developing faster integration algorithms and quantitatively evaluating the reconstruction precision.

REFERENCES

1. I. D. Yun, E. Jung, and S. Lee, "On the fast shape recovery technique using multiple ring lights," **30**, pp. 883–893, June 1997.
2. S. Nayar, A. Sanderson, L. Weiss, and D. Simon, "Specular surface inspection using structured highlight and gaussian images," *IEEE Trans. Robotics and Automation* **6**, pp. 208–218, April 1990.
3. S. Savarese and P. Perona, "Local analysis for 3d reconstruction of specular surfaces," in *IEEE Computer Vision and Pattern Recognition*, **2**, pp. 738–745, (Hawaii, USA), December 2001.
4. S. Savarese and P. Perona, "Local analysis for 3d reconstruction of specular surfaces: part ii," in *European Conference on Computer Vision*, pp. 759–774, (Copenhagen, Denmark), May 2002.
5. J. Y. Zheng and A. Murata, "Acquiring a complete 3d model from specular motion under the illumination of circular-shaped light sources," *IEEE Trans. Pattern Analysis and Machine Intelligence* **22**, pp. 913–920, August 2000.
6. R. Seulin, F. Merienne, and P. Gorria, "Simulation of specular surface imaging based on computer graphics : application on a vision inspection system," *EURASIP Journal on Applied Signal Processing* **2002**, pp. 649–658, July 2002.
7. D. Miyazaki, M. Kagesawa, and K. Ikeuchi, "Determining shapes of transparent objects from two polarization images," in *Proceedings of IAPR Workshop on Machine Vision Applications (MVA2002)*, pp. 26–31, December 2002.
8. D. Miyazaki, M. Kagesawa, and K. Ikeuchi, "Transparent surface modeling from a pair of polarization images," *IEEE Trans. Pattern Analysis and Machine Intelligence* **26(1)**, pp. 73–82, January 2004.
9. S. Rahmann, "Inferring 3d scene structure from a single polarization image," in *Conference on Polarization and Color Techniques in Industrial Inspection, volume 3826 of SPIE Proceedings*, pp. 22–33, June 99.
10. S. Rahmann and N. Canterakis, "Reconstruction of specular surfaces using polarization imaging," in *IEEE Computer Vision and Pattern Recognition (CVPR01), volume I, Kauai, USA*, pp. 149–155, December 2001.
11. L. B. Wolff, "Polarization-based material classification from specular reflection," *IEEE Trans. Pattern Analysis and Machine Intelligence* **12**, pp. 1059–1071, November 1990.
12. L. B. Wolff, "Polarization vision: a new sensory approach to image understanding," *Image and Vision Computing* **15**, pp. 81–93, February 1997.
13. L. B. Wolff and A. Andreou, "Polarization camera sensors," *Image and Vision Computing* **13**, pp. 497–510, August 1995.
14. L. B. Wolff and T. E. Boult, "Constraining object features using a polarization reflectance model," *IEEE Trans. Pattern Analysis and Machine Intelligence* **13(7)**, pp. 635–657, July 1991.
15. M. Born and E. Wolf, *Principles Of Optics*, Cambridge, 7 ed., 1999.
16. K. Ikeuchi and B. Horn, "Numerical shape from shading and occluding boundaries," *Artificial Intelligence* **17**, pp. 141–184, August 1981.